# Mapping Two Competing Grassland Species from a Low-Altitude Helium Balloon

Brenner Silva, *Member, IEEE,* Lukas Lehnert, Kristin Roos, Andreas Fries, Rütger Rollenbeck, Erwin Beck, and Jörg Bendix

***Abstract*—This paper describes a method of low-altitude remote sensing in combination with *in situ* measurements (leaf area, spectroscopy, and position) to monitor the postfire canopy recovery of two competing grassland species. The method was developed in the Andes of Ecuador, where a tethered balloon with a digital camera was deployed to record a time series of very high spatial resolution imagery (nominal resolution = 2 cm) of an experimental plot covered by two competing species: 1) the pasture grass, *Setaria sphacelata*; and 2) the invasive southern bracken, *Pteridium arachnoideum*. Image processing techniques were combined to solve geometric issues and construct high-quality mosaics for image classification. The semiautomatic and object-oriented classification method was based on geometrical and textural attributes of image segments and showed promising results for detecting the invasive bracken fern in *Setaria* pastures (performance by area under the curve, AUC = 0.88). Valuable insights are given into vegetation monitoring applications using unmanned aerial vehicles, which produces a time series of species-specific maps, including foliage projective cover (FPC) and leaf area index (LAI). This new method constitutes an important and accessible tool for ecological investigations of competing species in pastures and validation of remote sensing information on mountain environments.**

***Index Terms*—Field spectrometry, high spatial resolution photography, unmanned aerial vehicles (UAVs), vegetation mapping.**

## I. Introduction

THE Andes in southern Ecuador are a global hotspot of biodiversity [1], as is the Rio San Francisco valley, which breaches the eastward facing mountains of the Andean cordillera, connecting the provincial capitals of Loja and Zamora [2]. However, the high biodiversity harbored by the natural mountain rain forest is threatened by human activities, in particular by the conversion of forest to pasture. Satellite image interpretation has revealed that this problem is especially evident on the lower slopes of unprotected forest areas close to the main Loja–Zamora connection road [3]. On the cleared slopes, the pasture grass (*Setaria sphacelata*) is planted by farmers. Unfortunately, an aggressive weed, the southern bracken fern (*Pteridium arachnoideum*), is invading the pastures after recurrent burning, which is the primary pasture management method of the local population. Bracken outcompetes the pasture grass, and the pastures are abandoned, which increases the pressure to clear more of the natural forest [4]. A numerical growth model for both species was developed to determine the mechanism for the competitive dominance of bracken [5], [6]. However, to understand the spatial spread of bracken over time and spatially validate the results of the growth model, an effective tool is required to map the bracken and pasture grass coverage [e.g., in terms of the leaf area index (LAI)]. This tool must be adapted to the difficult conditions of a remote, partly inaccessible and steep high-mountain area. Satellite remote sensing might be an option, but spatial and temporal resolutions of the current operational sensors (e.g., Quickbird) are not sufficient to delineate the two competing species and the local cloud frequency ( > 80%) [7] severely complicates image acquisition from space.

In this context, low-altitude remote sensing (LARS) has the advantage to combine very-high spatial details useful for vegetation mapping on species [8], [9] and on plant community levels [10] with a near-real-time resolution below cloud cover. Depending on the system, investment and maintenance costs are rather marginal [11], particularly if the unmanned vehicle is equipped with light-weight, low-cost commercial digital cameras [12], [13]. Several approaches based on LARS vehicles are reported in the literature. For instance, deploying kite aerial photography [14] to classify vegetation in mountainous areas, using both supervised and unsupervised methods. Seven different species mixes were successfully delineated using balloon aerial photography based on a standard 28-mm nonmetric camera [15]. True-color balloon images can also be used either to single-point hyperspectral investigations [16] or to assess the accuracy of a hyperspectral image classification [17]. The latter usually requires LARS platforms with a very large payload [17]–[19]. Recent vegetation mapping approaches using small-frame cameras attached to unmanned aerial vehicles (UAVs) have proven a high accuracy of species detection through image classification [20]. However, the use of new radio-controlled UAV platforms (e.g., octocopters) is conditional to very stable flight conditions, which are rare in mountain regions, and has hitherto mostly been used in flat and accessible terrain. The advantage of the balloon-borne approach is the low cost of

Manuscript received January 13, 2013; revised January 06, 2014; accepted March 08, 2014. Date of publication May 21, 2014; date of current version August 21, 2014. This work was supported in part by the National German Research Foundation (DFG) under Grant BE1780/16-2, Grant BE473/38-1, and Grant BE473/38-2, in the scope of the DFG-Research Unit RU816 "Biodiversity and Sustainable Management of a Megadiverse Mountain Ecosystem in South Ecuador" and in part by the Brazilian Council of Technological and Scientific Development (CNPq) under Grant GDE 290033/2007-1. The work of B. Silva was supported in part by the Brazilian Council of Technological and Scientific Development (CNPq, GDE 290033/2007-1).

B. Silva, L. Lehnert, R. Rollenbeck, and J. Bendix are with the Faculty of Geography, Philipps University of Marburg, 32037 Marburg, Germany (e-mail: silvab@geo.uni-marburg.de; bendix@geo.uni-marburg.de).

K. Roos and E. Beck are with the Bayreuth Centre of Ecology and Environmental Research, University of Bayreuth, 95440 Bayreuth, Germany (e-mail: erwin.beck@uni-bayreuth.de).

A. Fries is with the Technical University of Loja, Calle París, 1101608 Loja, Ecuador.

Digital Object Identifier 10.1109/JSTARS.2014.2321896

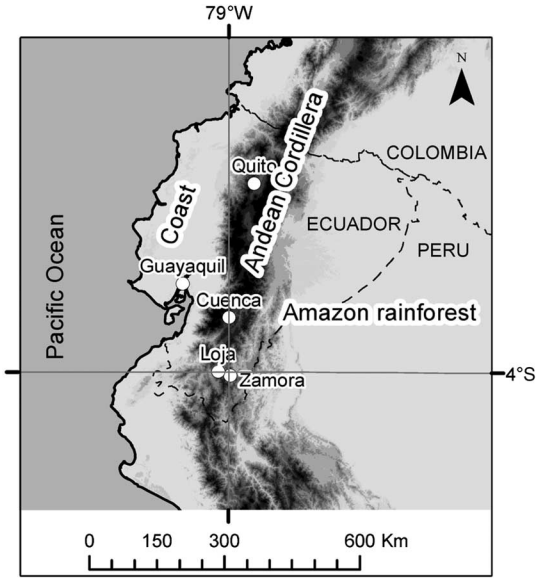


Fig. 1. Site location.

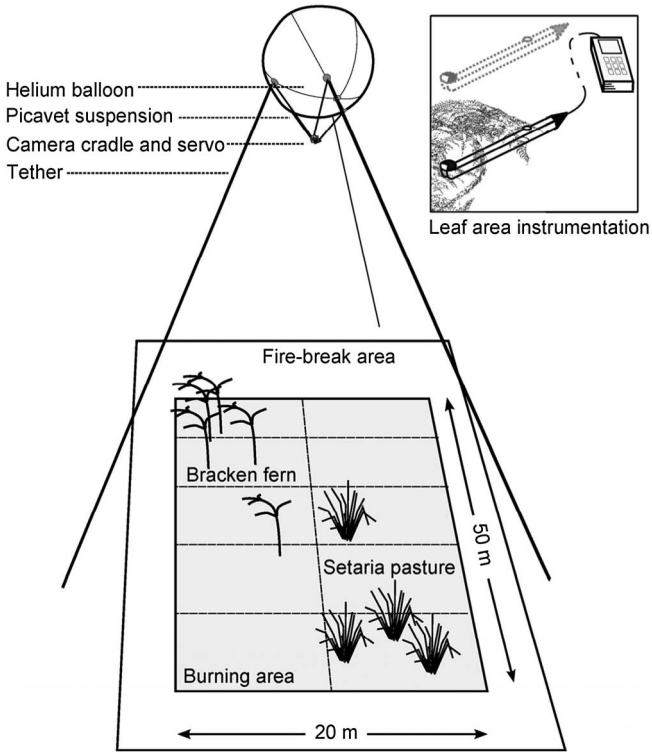


Fig. 2. Experimental setup.

platform and camera, which warrants a spatial image resolution of better than 2 cm from flight levels of 50–80 m [21].

The classification of different species based on airborne digital images is mostly conducted for trees using structural information [22], [23]. For scrubby and herbaceous vegetation, a combination of spectral and structural attributes is frequently used for this purpose. Landscape metrics based on balloon aerial photographs were applied to classify Mediterranean vegetation and assess fine-scale landscape fragmentation [24]. Investigation of vegetation patterns was conducted based on a digital Canon IXUS 500 camera using the supervised maximum likelihood method and spatial metrics, such as the mean patch size and density [25]. For instance, a database containing image examples of 19 weed species was constructed for an active shape model applicable to image classification [26]. Vegetation shape parameters, such as roundness, aspect, and perimeter, have been used for species image classification [27]. Shape and also texture measures have been successfully used to discriminate crop from weed plants [28], [29] and grass from shrubs [30]. With regard to bracken fern, several authors have stressed that discrimination might be facilitated by the specific reflectance properties of the fronds [31]–[35]. Efficient vegetation mapping approaches, using LARS and both spectral and spatial image properties, require continuous development and extensive application of this technique.

The objective of this paper is to describe a methodology to use balloon-borne, standard digital cameras to delineate two competing species, bracken and the pasture grass (*Setaria*). In the present methodology, the cameras provide noncalibrated images in the visible [VIS (RGB)] and near-infrared (NIR) spectral ranges, and the species cover was delineated in different vegetation stages due to pasture management, i.e., before and directly after burning, the common pasture management practice in the study area, and after regrowth of the plants. A time series of image mosaics is recorded and analyzed at different time steps to monitor changes in foliage projective cover (FPC). Finally, FPC is converted into LAI using species-specific allometric functions.

The paper is structured as follows. First, we present the study site, balloon-borne photo acquisition, and ground measurements. Then, we describe the developed image processing method, which includes bundle adjustment, terrain surface reconstruction, geometric rectification, image enhancement, segmentation, and classification of FPC. FPC is then blended with ground measurements to produce LAI maps. Finally, validation of the produced maps is presented using independent ground observations of FPC and LAI.

## II. Study Area, Data, and Methods

### A. Study Area

The current project was conducted in the framework of an interdisciplinary, ecological research project situated at the eastern slopes of the eastern Andean cordillera of southeast Ecuador in the San Francisco River Valley (Fig. 1) [2]. To investigate the competition between pasture grass and bracken, an experimental site was established for an ecological fire experiment (Fig. 2), which was used to develop and test the low-cost LARS methodology presented in this work. The plot is $50 \times 20$ m and has a slope inclination of 38°. It is located at S $3°58'18''$ (latitude), W $79°4'45''$ (longitude) at 2107 m above sea level. The plot was mostly covered by the common pasture grass (*Setaria sphacelata*), which was planted in rows, and the invasive southern bracken (*P. arachnoideum*). The area was closed to grazing for 2 years and was completely burned in September 2008 and again in November 2009 to mimic the current pasture management practice of recurrent burning and to evaluate its impact on vegetation succession. We used the balloon platform to monitor vegetation succession after November 2009.

TABLE I
SUMMARY OF IMAGE AND ANCILLARY DATA

| Balloon flight | | | | | Ground LAI | |
|---|---|---|---|---|---|---|
| Date | MAB | Mode | Shots | Tiles | Date | MAB |
| 31-10-2009 | –1 | VIS | 156 | 9 | 15.03.2008 | –1 |
| | | NIR | 256 | 10 | 18.09.2008 | –1 |
| 8-11-2009 | 0 | VIS | 166 | 13 | 28.09.2008 | 0 |
| | | NIR | 87 | 9 | 1.12.2008 | 2 |
| 6-12-2009 | 1 | VIS | 161 | 10 | 14.1.2009 | 4 |
| | | NIR | 144 | 8 | 11.3.2009 | 6 |
| 14-03-2010 | 4 | VIS | 332 | 3 | 24.10.2009 | –1 |
| | | NIR | 149 | 8 | 10.11.2009 | 0 |
| 27-10-2010 | 12 | VIS | 535 | 4 | 15.5.2010 | 6 |
| | | NIR | 185 | 4 | 23.10.2010 | 12 |

The date of the flight is shown in the leftmost column. "MAB" is the number of months after burning. "Mode" is the camera mode (VIS, visible; NIR, near infrared). "Shots" is the number of images captured per flight. "Tiles" refers to the selected image tiles from shots. LAI (ground LAI) measurements ($n = 40$ per date and species) are shown by date and "MAB." Summary of the DGPS survey is shown in the rightmost column.

### B. Balloon Photos and Ancillary Data

Aerial images were captured with a standard digital camera (Ixus-90; Canon, Inc., Tokyo, Japan) mounted on a tethered, $3\ \mathrm{m}^3$ helium balloon, which can lift a 1.3-kg payload. The camera was attached to the balloon with an automatic shutter using a light metal frame and a cross-wired picavet [20]. A second camera, modified with an infrared transmitting filter RG715 (SCHOTT AG, Mainz, Germany), was deployed on a consecutive flight to obtain images in the NIR. The objective with 35-mm focal length (135 film equivalent) records images of $2736 \times 3648$ pixels, which, at a height of 35 m, corresponds to a field of view of $26 \times 34$ m, yielding a ground resolution of 1 cm. The total cost of the platform and camera was US$1200 (€ 900). During each flight, the automatic shutter released one photo every 10 s while the tethered balloon was towed over the plot. Image acquisition was mostly conducted under partly cloudy conditions. Due to frequent air turbulences causing temporary camera shake an average of 180 photos per flight had to be taken to warrant full image coverage of the experimental plot with high-quality imagery. Each flight took no more than 2 h between the acquisition of the first and last photo for both RGB and NIR cameras. Flight time was fixed between 11:00 and 14:00 LT due to best weather conditions and in order to guarantee comparable illumination conditions for all datasets. After each flight, a visual selection of photos was necessary to include only high-quality "image tiles" in the processing workflow (see Section II-C). Table I summarizes the images and ancillary data used.

*1) Ground Control Points:* To facilitate geometric correction, a net of Differential Global Positioning System (DGPS)-located landmarks ($10 \times 10$ m) was installed at canopy height ($\sim 50$ cm above ground). The collected DGPS data ($n = 36$ points) were processed with a mean horizontal and vertical precision of 0.76 and 1.36 m, respectively. The DGPS data were used for the rectification of the balloon imagery by providing real-world coordinates in the construction of a digital elevation model (DEM), which in turn resulted from the surface reconstruction (see Section II-C2).

*2) LAI Data:* LAI was measured based on near-hemispherical light transmittance with a LI-COR LAI-2000 plant canopy analyzer (LI-COR, Inc., Lincoln, NE, USA). A measuring protocol [36] was used with a view restrictor (45 °) under diffuse light conditions to avoid multiple scattering. Five sample areas (each $1\ \mathrm{m}^2$) predominantly occupied by only one species (bracken or *Setaria*) were marked on the ground within a $25\text{-m}^2$ area. Five LAI measurement campaigns were conducted for each sample area for a total of 40 LAI records for each species per sampling date. Light transmittance was also used to measure FPC. We conducted measurements and the derivation of species specific LAI to FPC conversion parameters to allow a proper validation of FPC and LAI, which could be obtained from imagery.

*3) Field Spectroscopy:* Calibrated reflectance data were collected with the field spectrometer (Handyspec-14, Tec5 AG, Germany) using a fixed mounting [37]. For a direct comparison, photos were simultaneously recorded with the balloon digital camera (IXUS-95, Canon Inc.). In total, 18 samples of fresh green leaves of bracken and *Setaria* were recorded. The spectroscopy data were integrated to the corresponding spectral ranges of the photos (blue 450–520 nm, green 520–600 nm, red 630–900 nm, and NIR 760–900 nm) and used to analyze the spectral traits (VIS and NIR) from the noncalibrated digital cameras.

### C. Image Processing

The workflow can be divided into the three consecutive processing steps as separated by dotted lines in Fig. 3. The first processing step (Fig. 3, left) is the construction of the image mosaic. First, overlapping images were used to reconstruct the surface and to orthorectify the contrast normalized image tiles onto a mosaic grid. In the second processing step (Fig. 3, center), the single VIS bands (blue, green, and red) were enhanced, segmented, and classified into bracken and pasture grass based on texture attributes gained from the NIR and RGB images as well as geometric indices. Finally, visual interpretation was performed for validation of the classification. The third processing step (Fig. 3, right) is the conversion of FPC to LAI, which consists of a single step. The *in situ* acquired LAI dataset was bisected and used to derive the allometric conversion function and to validate the image-derived FPC and LAI values. We used the open source software "Bundler" [38], "GRASS" [39], "SAGA" [40], and "gbm" R-package [41], and customized them for automation of the processing steps (Fig. 3) using R and Python languages.

The processing steps 1–3 include the following procedures.

*1) Digital Values Analysis and Images Selection:* Since the digital cameras were not spectrally calibrated, we analyzed the relative differences in digital values between our main targets (bracken and *Setaria*) using a calibrated field spectrometer (see Section II-B3). The purpose of this operation is to retain a realistic spectral contrast in digital values, which is necessary in the classification step, since this is also based on optical species traits (see Section II-C6). The spectral data were used as a reference to control the mosaics of all the flights (see Section III-F).

Visual inspection of the whole image stack was conducted to exclude images with limited geometric quality due to camera

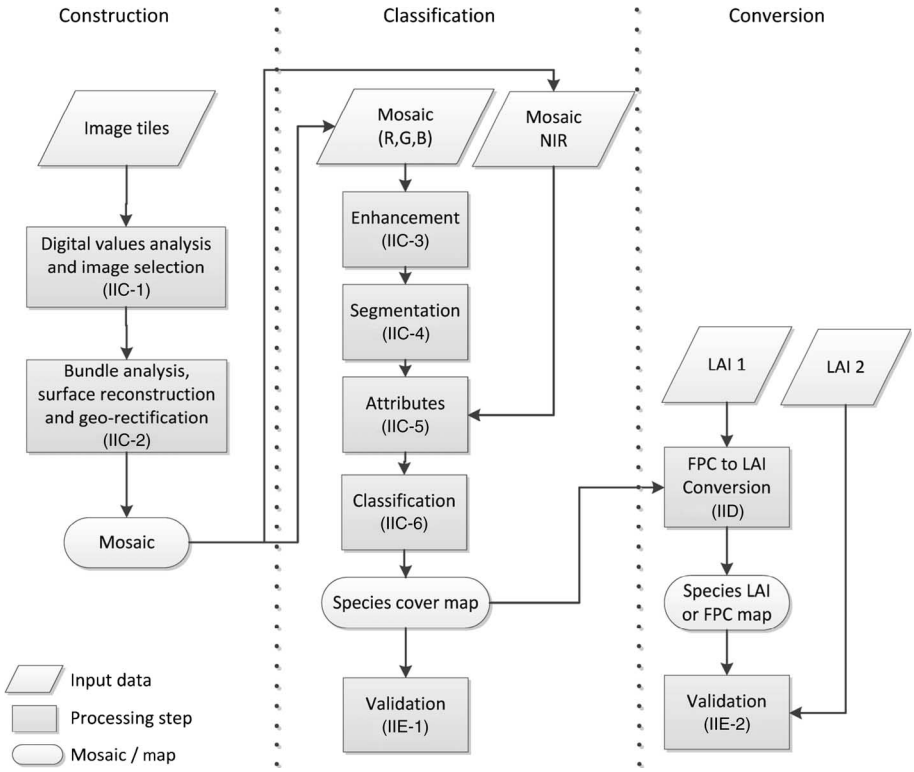


Fig. 3. Main processing workflow. The numbers in brackets refer to the corresponding sections in the text.

shakes and to select a reference image for contrast balancing. Two sets of photos were identified for processing. The first contained very-high overlapping (larger than three times the entire plot area) and sufficient spatial details for automatic bundle adjustment (see Section II-C2). The second is a subset of the first, containing best quality photos (spatial and contrast) with full coverage of the plot area. To the latter, a contrast matching method [42] was applied before orthorectification. A total of 50 pixel values equally distributed across these image tiles were extracted for green leaves of bracken and *Setaria* and compared with the field spectroscopy data. This comparison was used to assure whether the spectral contrast between species was available for classification of the final mosaic.

*2) Bundle Adjustment, Surface Reconstruction, and Geometric Rectification:* We applied the technique of bundle adjustment and surface reconstruction based on a "Structure from Motion algorithm" (SfM) [43], which is fully automatic using "Bundler" [38]. The result is a three-dimensional (3-D) point cloud in camera coordinates. These coordinates were transformed to real-world coordinates using the Helmert transformation and the DGPS-derived landmark coordinates as ground control points (GCPs). From the dense 3-D point cloud, a DEM was constructed. The SfM surface reconstruction is based on scale invariant transformation, which is applied to find similar features in image pairs. The two-dimensional (2-D) camera coordinates of matching features are then used to calculate the camera position and 3-D coordinates from corresponding 2-D camera coordinates [44]. The matching features found, their corresponding 2-D and 3-D coordinates, were used as GCPs for geometric rectification. The orthorectification algorithm available in the "GRASS" software was used [39], which considers the DEM and camera-orientation parameters for differential rectification of each image [45]. Only the selected images with full area coverage were used to generate the final image mosaic of the experimental plot area (Fig. 4). Camera-orientation parameters summarized by flight were used to analyze potential errors in the classification step due to remaining geometric inaccuracies (Table II). Visual inspection of image features common to all flights was used to calculate an overall root mean square error (RMSE) of the spatial position accuracy over time.

*3) Enhancement:* To apply single-band-based segmentation procedures (Section II-C4) without losing the spectral information of the RGB photo, a band difference image (*eRGB*) was calculated as follows to enhance green vegetation:

$$eRGB = 2 \times g - r - b \tag{1}$$

where $g$, $r$, and $b$ are the digital values in green, red, and blue channels, respectively. The *eRGB* image is similar to the NIR-mosaic, but richer in contrast. The poor contrast of the NIR band is due to lower sensitivity of CCD sensors in the NIR range, which would lead to poor segmentation results in terms of geometrical details of foliage. Thus, the enhanced image (*eRGB*) was used for segmentation, while the NIR mosaic was used to fed the classification (Section II-C5), thus allowing to use the already known spectral differences in NIR reflectance between our considered species [5], [31]–[35].

*4) Segmentation:* Image segmentation by seeded region growing was applied to the final mosaics in two successive steps: 1) the seeding by application of cutoff values and 2) the pouring segmentation or region growing. This procedure is similar to that used to detect individual tree crowns in LiDAR

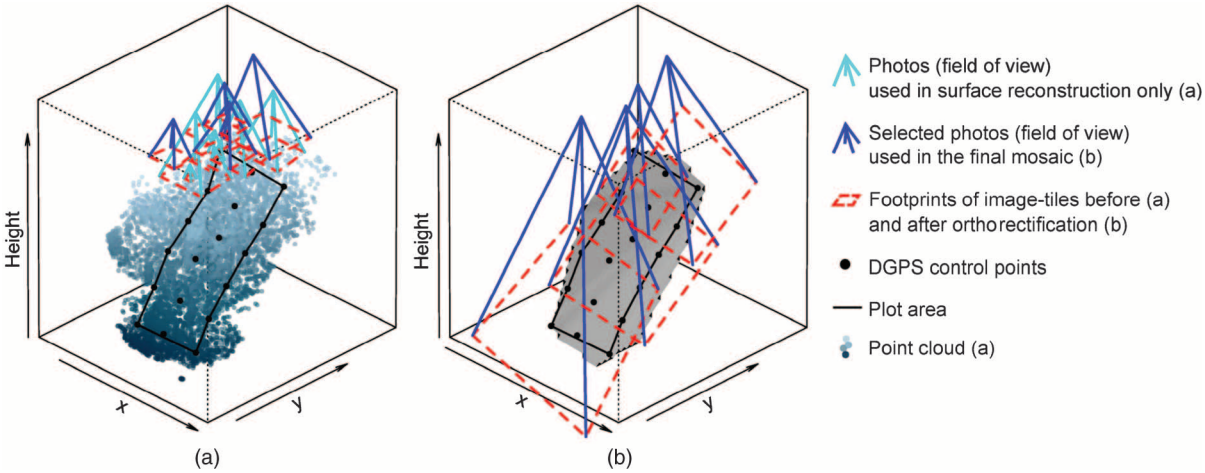


Fig. 4. Acquisition geometry for flight 27-10-2010 illustrating the initial set of captured photos (a), which were used in the construction of the point cloud and (b) the geometric rectification onto the elevation model.

TABLE II
SUMMARY OF ACQUISITION, *POST HOC* GEOMETRY, AND SPATIAL ACCURACY

| Date | Max. roll | Max. pitch | Mean height | Geo. RMSE |
|---|---|---|---|---|
| 31-10-2009 | 22 | 16 | 21 | 0.10 |
| 8-11-2009 | 16 | 9 | 18 | 0.08 |
| 6-12-2009 | 19 | 28 | 20 | 0.09 |
| 14-03-2010 | 17 | 8 | 23.7 | 0.10 |
| 27-10-2010 | –19.1 | –4.7 | 23.9 | 0.07 |
| Overall | | | | 0.10 |

*Post hoc* geometry is represented by maximum roll, maximum pitch, and mean height, while spatial accuracy by the RMSE after geo-rectification (Geo. RMSE). Summary is for VIS and NIR image tiles.

data, where the seeds are given by the local maxima in the canopy point cloud [46]. However, in the *eRGB* image, the green foliage is represented by high digital values, and the highest values are mostly central to each individual plant. So, from higher to lower *eRGB* values, cutoff values (*si*) were successively taken to obtain image segments, which were used as seeds for region growing. Segments with pixel values higher than *si* were used as seeds for region growing. Region growing enlarged the segments by iteratively choosing a similarity threshold between neighboring pixels and seeds, as implemented in the software "SAGA" [40]. Both segmentation steps were iteratively conducted reducing the cutoff value ($si + 1 = si - 25$) until the whole plant cover in the image was segmented. The successive thresholding followed by region growing permitted to avoid over-segmentation. Resulting image segments were vectorized and used to calculate the attributes table.

*5) Attributes Calculation:* Three sets of attributes representing geometry and texture (NIR and *eRGB*) were calculated from each image segment. Geometry attributes used were "area," "perimeter," "compactness," "circularity," "elongatedness," "circularity ratio," "ellipticity index," "shape factor," and "grain shape index." For the equations of the geometry attributes, the reader may refer to [47]. Image texture was derived from gray-level co-occurrence matrices [48], which were constructed from *eRGB* segments and corresponding parts in NIR images. The set of texture attributes was composed by the following textural features: "energy," "entropy," "correlation," "inverse difference moment," "inertia," "cluster prominence," "cluster shade," "Haralick's correlation," "variance," "difference entropy," "difference variance," "information of correlation 1," and "information of correlation 2." The reader should refer to [48] for corresponding equations to derive the texture attributes. All geometry and texture attributes together composed the attributes table used in the classification.

*6) Classification:* Since the plant cover was composed of two species only ( $> 97\%$), a supervised classification based on the attributes table was applied to detect "bracken" and "*Setaria*" pasture. In the classification, we used a boosted regression tree (BRT) model [49] using the "gbm" package [41] and a custom made code [50] in R-language [51]. Training data were segments within two sample areas of $100\ \mathrm{m}^2$ size, where bracken and *Setaria* segments were visually identified. Their corresponding attributes were used for training the BRT model. The BRT model was fitted using a low learning rate ($= 0.005$), a moderate tree complexity ($= 5$), and the number of trees which resulted in the best predictive power. The final result is the probability of each segment to pertain to the class "bracken." A separation threshold for the definition of the two classes (bracken and *Setaria*) was chosen based on the highest hit rate on the validation area (see Section II-E1).

### D. Conversion of FPC to LAI

To obtain the LAI from the classified images, ground measurements of light transmittance were used to calculate species-specific relationship between LAI and the FPC, which is given by

$$FPC = 1 - G \tag{2}$$

where $G$ is the diffuse light penetration perpendicular to the ground which is equal to the gap fraction. While LAI is based on hemispheric gap fractions, $G$ is the transmittance projected to a horizontal plane [36]. Thus, foliage orientation was considered to calculate a direct relationship between FPC to LAI

$$LAI = -\ln(a - FPC) \times b \tag{3}$$

where $a$ and $b$ are coefficients to be fitted to species-specific LAI and FPC data. These parameters are used to explain the species-specific divergence in the LAI to FPC relation due to the predominant leaf angle of each species [5]. Because of measurement uncertainties in areas with a sparse plant cover or the extremes in areas of closed vegetation cover, the considered range of FPC was limited to $0.15 < \mathrm{FPC} < 0.95$. In addition, we assume LAI equals green-LAI for the first year after burning. Previous investigations [4] in neighboring areas showed an average lifespan of *Setaria* leaves and bracken fronds of 11 and 8 months, respectively.

### E. Validation

*1) Validation of Classification:* Validation maps were constructed for two sample areas ($100\,\mathrm{m}^2$ size, excluding training sites) by visual identification of bracken individuals in the RGB photomosaic. To assess the classification accuracy, we calculated the area under the curve (AUC) of the receiver operating characteristic (ROC) accuracy method [52]. The area under the ROC curve (AUC) expresses the general probability of a given detection to be correct in the space of all occurrences of hit rate (h) in relation with the false alarm rate ($f$), which are given by

$$h = p/(p+n) \tag{4}$$

$$f = q/(q+m) \tag{5}$$

where $p$ (true positive) is the fraction of the map assigned to a class (bracken or *Setaria*), which is in agreement with automatic and visual selection of bracken entities. Similarly, $m$ (true negative) is the fraction correctly not assigned to bracken, thus to *Setaria*. The variables expressing disagreements are $q$ (false positive) and $n$ (false negative). The first computes the fraction of bracken incorrectly detected by the automatic classification, but not by the visual interpretation, while n computes the opposite. The AUC is calculated using the Wilcoxon's statistic method [52]. Reasonable performance is obtained with values higher than 0.7, while very good performances are obtained with AUC higher than 0.9 [53]. The final map is given by the selection of a decision threshold, which results in the pair of highest h and lowest p coordinates.

*2) Validation of LAI Maps:* We used the ground measurements (FPC and LAI) to validate the final FPC maps. From the FPC maps, two extents ($5\ \mathrm{m} \times 5\ \mathrm{m}$) containing the ground sample areas were extracted and converted to LAI (see Section III-G). Mean values were compared with ground data, either directly or after linear interpolation in time. In the validation of LAI, the RMSE was calculated by averaging the square of the difference between LAI measurements and values derived from FPC maps.

## III. Results

### A. Image Acquisition

A time series of balloon-borne aerial photos from the experimental plot was acquired, processed into image mosaics, and classified to obtain the projective cover of bracken fern and *Setaria* pasture. A summary of acquisition parameters is given in Table II. With exception of 14-03-2010, the relatively high numbers of photos (from 8 to 13) are due to either obliquity or recording at low height. For instance, the mosaic of 31-10-2009 is composed of nine tiles and has maximum obliquity (roll or pitch) of 22 ° and a mean height of 21 m. The mosaic of 14-03-2010 has a maximum obliquity of 17 ° at 23.7 m mean height.

### B. Geometric Processing

The acquisition geometry is an indicator of spatial accuracy and mapping quality. The overall displacement of the time series was 10.2 cm, which is higher than the nominal resolution (2 cm). However, the time series was considered adequate to calculate and analyze the projected cover in a grid resolution of 1 m. The maximum displacement between NIR and RGB was $\sim 8\ \mathrm{cm}$. Thus, in the classification step (see Section II-C6), the assumption of "topological inclusion" of NIR image features to the first-image segments mostly depended on the size of objects. Displacement values were mainly due to parallax effects on canopy cover. Therefore, the higher the number of tiles or the maximum roll or pitch (Table II), the lower the quality and spatial accuracy of the mosaic. This concept holds for the calculated height above ground, which is inversely correlated to the number of photo tiles, but, in this case, increasing the ground sampling distance. In general, the mapping quality for the study site slightly decreased from the center to the extreme north and south part of the plot.

### C. Relationship Between Brightness and Reflectance

Fig. 5 shows the reflectance integrated for the VIS (RGB) and NIR channels of green leaves of bracken and *Setaria*. As observed in the spectroscopy [Fig. 5(a)], *Setaria* has higher values in RGB but slightly lower in the NIR compared to bracken. This relationship is reproduced by the noncalibrated camera using the same measuring setup as for spectroscopy [Fig. 5(b)]. As observed in mosaic 27-10-2010, the relative difference between *Setaria* and bracken are similar [Fig. 5(c)]. The contrast matching led to relatively lower values in the red channel and higher variance in the NIR channels, respectively. Lower red values of green leaves higher variability in the NIR reflectance due to illumination geometry can be used to explain the reduced contrast in those channels in the final mosaic [Fig. 5(c)]. However, *Setaria* is still brighter in the VIS (especially in the blue and green channels) and tends to be darker than bracken in the NIR channel. In general, variance increased from spectroscopy to noncalibrated cameras but the relative differences between bracken and *Setaria* leaves are maintained, at least using average values.

### D. Segmentation and Classification

Relative to the RGB image [Fig. 6(a)], a high contrast was observed between green canopies (bright) and the background (dark) after image transformation [Fig. 6(b)]. These dense, covered areas resulted in the construction of seed areas or seed pixels in the first segmentation iteration [Fig. 6(c)]. Partially overlaying individuals were separated only if digital numbers of all features differed by more than the cutoff value, which was the case of fern fronds, in contrast to *Setaria* leaves. Within *Setaria*

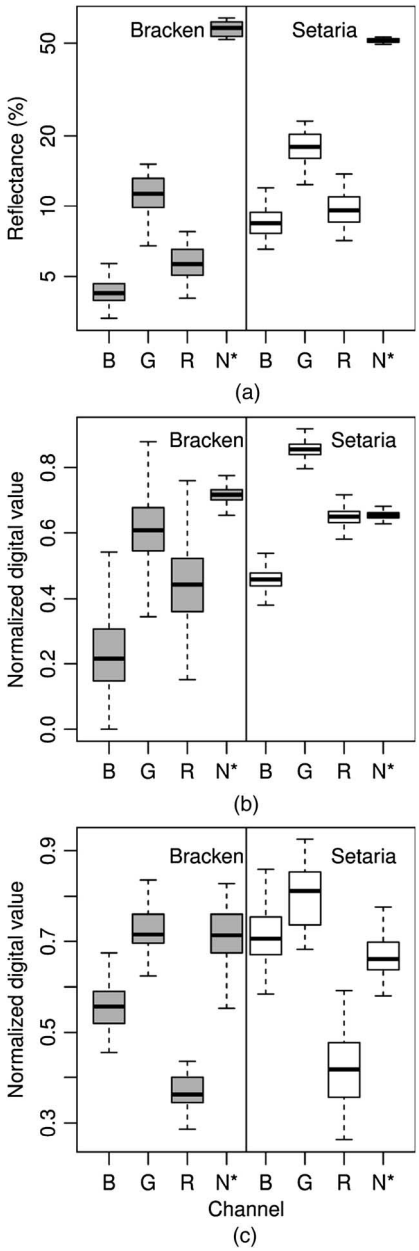


Fig. 5. Reflectance of green leaves in red (R), green (G), blue (B), and NIR channels by (a) field spectroscopy, (b) camera digital values measured using spectroscopy setup, and (c) camera digital values from the image mosaic of 27-10-2010. In (b) and (c), note that NIR values are not calibrated in relation to RGB, which is not required in a classification approach.

canopy, the contrast was higher than within that of bracken, which led to more than one segment per grass bunch [Fig. 6(d)]. Fig. 6 also shows the NIR image with the classified segments as overlay. The small displacement between NIR and *eRGB* images can be observed. Despite that, in the case of Fig. 6, image of 27-10-2010, the BRT-classification pointed the NIR-derived attribute values as the most important for classification. It shows that the topological inclusion still holds despite the spatial displacement between the NIR image and *eRGB*-derived segments. In general, "texture" contributed more to classification than "geometry." Geometry attributes were significantly important in the two dates of growing phase after fire, which is reflected in the validation.

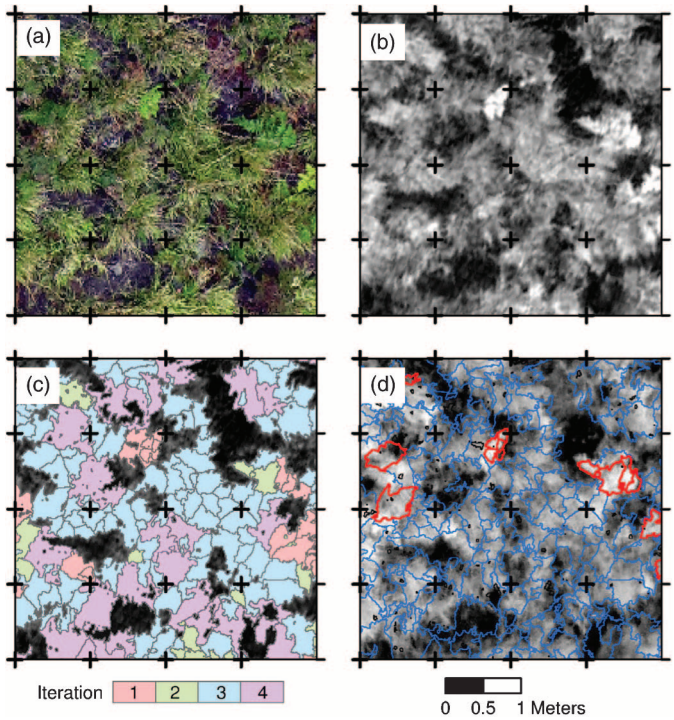


Fig. 6. Aerial image mosaic (a) before and (b) after enhancement and (c) after segmentation. In (c), objects resulting from four consecutive segmentation steps are shown. In (d), the classified segments overlay the NIR image (bracken fern is in red; *Setaria* is in blue).

The relative importance of each segment attribute in the classification and for each flight was analyzed in terms of the BRT model fitting. The relative importance is the sum of all improvements given by splits in the BRT model, which were determined by the attribute [54]. To avoid a plethora of figures, we used the relative importance of the top ten variables to summarize the four flights (Fig. 7). The foliage recovery can be used to explain changes observed in the relative importance of variables derived from geometry *eRGB* and NIR texture during vegetation recovery. Under initial conditions [before burning, Fig. 7(a)], all attributes have similar importance. The *eRGB* (light gray), NIR (gray), and "geometry" (dark) attributes alternate in the top ten positions, which can be seen here as characteristic of a stage of at least 2 years of regeneration after planting the grass. In the first month of recovery after the fire [Fig. 7(b)], the "texture" attributes of *eRGB* contain most information for distinguishing both species, and the dominance of grass bunches lead to a low relative importance of "geometry" attributes. After 3 months [Fig. 7(c)], fern leaves are completely unfolded but are still isolated from grass bunches and among each other. Since then, the "geometry" attributes reveal important information for classification, comparable to NIR. A year after the first flight [Fig. 7(d)], the foliage closure almost reaches the complete closure. In this case, the separation of bracken from grasses in the NIR becomes notable. Clumping effects, as used to explain higher contrast within grass bunches, seem to neutralize "geometry" attributes after 1 year, while equally aged leaves of bracken and *Setaria* are better separated by their spectral traits [Fig. 7(d)]. Differences in "geometry" were more important after longer regeneration time, as shown in the first flight [Fig. 7(a)]. The

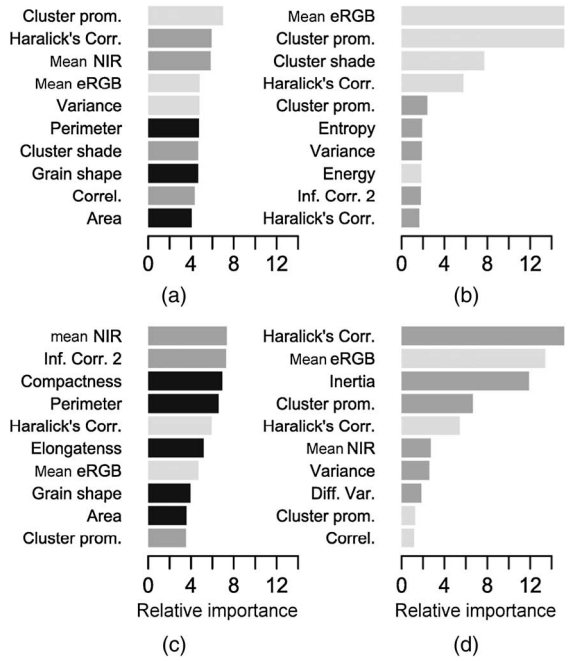


Fig. 7. Relative importance (12 = high) of the top 10 important segment attributes used as predictors in BRT classification. Light gray bars indicate attributes derived from the enhanced information (*eRGB*), medium gray belongs to the same class of attributes but derived from the NIR image, and dark bars represent "geometry" attributes. Attribute names are partially abbreviated from that mentioned in Section II-C5.

rearrangement of attributes provided by the BRT model fitting was important for the overall classification performance.

### *E. Validation of Classification*

Classification results were considered reasonable for the image before burning (31-10-2009) and 1 year after (27-10-2010), which results in AUC equal to 0.81 and 0.83, respectively. In both situations, the dense canopy of *Setaria* resulted in small areas of reflection spots within the canopy in the enhance image. These areas caused confusion with bracken segments. Four weeks after burning (06-12-2009), isolated bracken segments were much easier to classify (AUC = 0.99). Similar results were obtained 4 months later (14-03-2010), when AUC = 0.91. The general classification performance is relatively high (AUC = 0.88 in average), which corresponds to the detection of bracken fronds in a *Setaria* pasture.

### *F. Maps of Vegetation Development*

The time series of images and canopy cover classification is presented in Fig. 8. Image mosaics are shown in line (a). Line (b) shows the species canopy maps. Lines (c) and (d) show the maps of FPC for *Setaria* and bracken, respectively. The plot was completely burned in November 2009 [column (ii)]. After 1 month, the recovery of the *Setaria* canopy was faster than that of bracken [column (iii)]. Field observations showed that the bracken area was occupied by small and sparse unfolded fronds. However, the status after 4 months [column (iv)] shows a more intensive recovery of bracken in the medium term (prior 3 months). After 1 year [column (v)], the canopy recovered to the preburn closure status, but with differently distributed

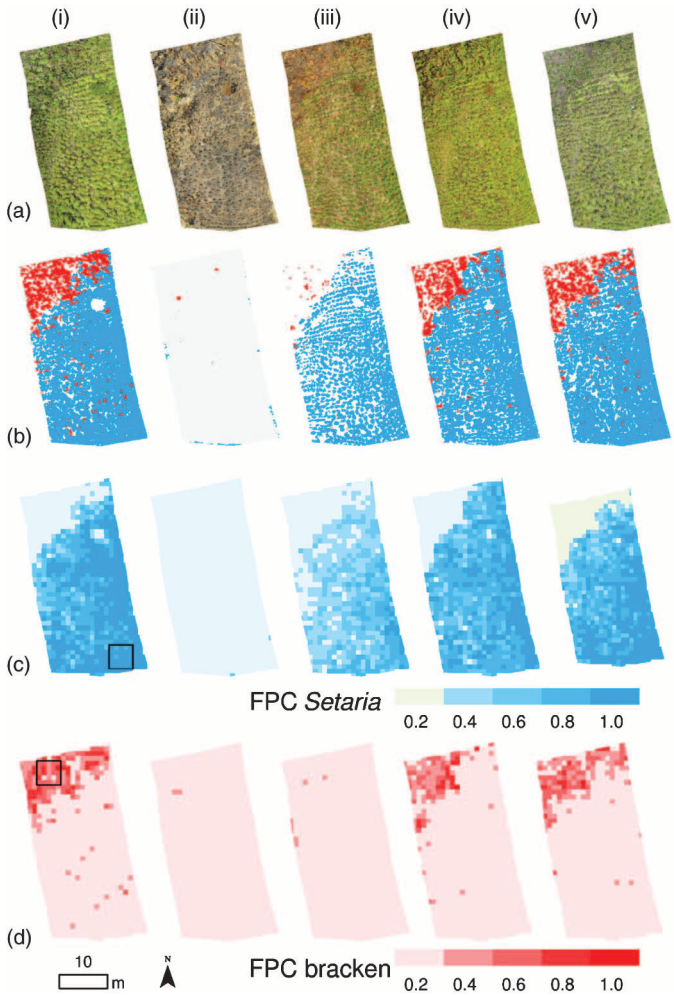


Fig. 8. Time series of five dates for the experimental plot. From left to right: time sequence corresponding to balloon flights. From top to bottom: image mosaics, cover maps, and FPC for *Setaria* (blue) and bracken (red). Areas of ground LAI measurements are depicted in the bottom left FPC maps.

bracken fronds in the *Setaria* (south) area. This pattern suggests the sprouting of fronds from the existing living rhizomes, which are present in the whole area.

### *G. Conversion of FPC to LAI*

Fig. 9 shows the relationship between ground FPC and LAI data and the conversion function used to calculate the LAI values from FPC values. The more rapid exponential increase in *Setaria* LAI values is due to more vertical leaves in the developed foliage in comparison to bracken.

### *H. Validation of LAI Data*

Fig. 10 shows the observed LAI values through time, as derived from ground measurements (LAI ground) and FPC maps (LAI balloon, based on functions in Fig. 9). Time is normalized to months after the date of burning ("MAB" in Table I). In general, FPC and LAI-values were underestimated with the species-cover maps derived from balloon photos. One reason is the overlap of leaves, which is not completely resolved by the conversion function. This effect was stronger in the bracken canopy [Fig. 10(a) and (b)] and was more pronounced in the first

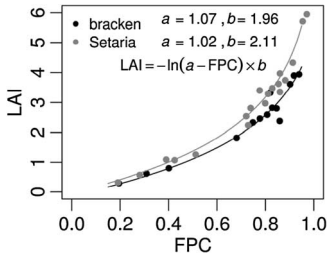


Fig. 9. Relationship between ground FPC and LAI data, and conversion function calculated for bracken and *Setaria* foliages.

months (1–6). The presence of unfolded fronds (month 2) and sparse foliage (months 4 and 6) reduced the average area in the balloon-derived FPC and, thus, LAI. For instance, if the maximum FPC value is used, the RMSE decreases to 0.83 for bracken.

The rapid increase in *Setaria* foliage after burning was observed by both ground and balloon data. The variability observed in the averages of *Setaria* LAI ground data after burning is most likely due to nonconfirmed assumptions made for LAI measurements (see Section II-B2). However, the deviation shows that the measurements from months 2, 4, and 6 can be considered at the same level, which means that the *Setaria* foliage is already developed after 2 months. To summarize, a better agreement was found for *Setaria* foliage in comparison to bracken, which is expressed by the lower RMSE [Fig. 10(b) and (d)].

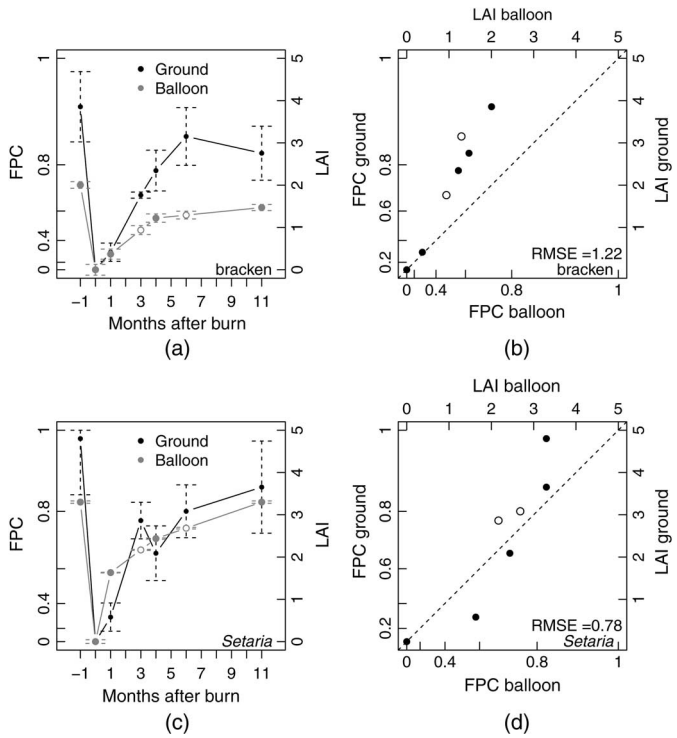


Fig. 10. Comparison of FPC and derived LAI values in time [left (a) and (c)] and between ground measurements of FPC and LAI values derived from balloon photography [right, (b) and (d)]. Open circles are linearly interpolated values.

## IV. Discussion

Compared to other approaches from the literature, the present work contributes with advances in mapping and monitoring grassland competing species employing a cost-effective balloon system. Knowledge gained in the present approach can be used to overcome the influence of very-high-resolution phenomena, such as frond shading, acquisition geometry, and the RGB-NIR displacement. For instance, the automatic construction of a high-resolution DEM was essential for the geometric rectification, thus allowing the use of a dual-camera system. In addition, texture information from both cameras was combined in the attribute table based on the extracted segments (plant individuals). Segmentation by successive seeding allowed the categorization of leaves and fronds under clumping, overlaying leaves and partial shadowing. This same procedure also helped to minimize the still existing influence of the acquisition geometry, as well as illumination artifacts in the green canopy. Grid-based metrics (e.g., NIR values) maintained physical properties of the segments and were very useful in the classification, especially in the first year of recovery.

Vegetation maps were produced using automatic or semiautomatic procedures. This shows the potential and flexibility of open-source tools, which could be customized and combined in the present method. However, manual intervention was still required to initialize or to evaluate intermediate steps and to a final edition of the species maps. Taking the semiautomatic classification as a starting point, final edition of vegetation maps was achieved in 4 h of labor. In comparison with a completely visual interpretation, this represents a significant gain in terms of time, since 4 h of labor was required to edit an area of only $25\ \mathrm{m}^2$, used in the validation of classification results. Considering a future operational application, the present work pointed the good capability of detecting bracken and grass canopies using flexible tools and the cost-effective balloon-borne system.

Observations in a time series using the method proposed here are new to the literature. Regarding bracken fern and *Setaria* pasture, differences were observed regarding image segmentation and classification during canopy recovery. Due to horizontal-shaped fronds and high infrared reflection, bracken fronds were relative easily detected in the *Setaria* pasture. In a more general application, good performance can also be expected in the time after burning. However, ancillary information on different recovery times and regeneration phases (lifespan) is essential to explain classification results or to even develop a more complex classification approach (e.g., using artificial neural network). In addition, the projective cover maps (see Section III-F) showed a rapid recovery of *Setaria* in comparison with bracken. The observed canopy recovery might be due to the absence of cattle browsing, which would affect *Setaria* pasture more than bracken fern. Furthermore, information on fire severity, which can be higher in a wider and uncontrolled fire, is equally important for operation in a larger experiment. Fire severity could be assessed in field or by remote sensing. The latter requires data in short-wave infrared, which are not available using standard CCD-sensors. Finally, LAI maps can be directly used in numerical growth models. To be mentioned, numerical growth models rely on a consistent time series of data, once uncertainties (e.g., in biomass productivity) can be solved from on time-step to the next.

The present methodology can be easily adapted for other plot monitoring projects. We suggest five points for improvements:

1) simultaneous RGB-NIR imaging could improve segmentation, though a proper fusion technique should be investigated; 2) a more stable platform can be deployed to avoid wind-gust, thus optimizing image acquisition; 3) overlapping images are still required to surface reconstruction, which is not only essential to image rectification, but can also be used to derive important information in the time series (e.g., height above ground or projected cover); 4) the plant canopy analyzer can be deployed to adjust the conversion function for other species, but the instrument operator should be aware of the effect of sparse canopies on the measurements; and 5) the automatic classification, especially of sparse fronds, can be improved by including spatial metrics at the plot level, such as distance to the next vegetation segment, or to a previously existent one in the time series. Additional payload (e.g., multispectral cameras, inertial measurement unit, and GPS) could increase classification performance, but also requires higher costs and a more complex logistic at the monitoring site.

## V. Conclusion

A methodology for recording and processing low-altitude balloon-borne photos was developed, focusing on the occurrence of plant individuals (bracken fronds and grass bunches) on a plot scale. We showed that a cost-effective platform can be used to record quality image mosaics, which can be processed and classified using semiautomatic and procedures. Robust tools available for processing aerial imagery (e.g., surface reconstruction) allowed high-quality geometric rectification in a time series of image-pairs (VIS and NIR). Classification was based on geometric and textural attributes of image segments and showed promising results for monitoring invasive weeds and canopy recovery after fire. The rearrangement of attributes in relative importance of the BRT-model allowed not only good classification performance, but also lead to important insights related to species-specific canopy recovery. Validation of mapping results included measurements of projected cover, which can also be used to obtain species-specific LAI maps. The present method can be easily extended for other grassland areas and species. We conclude that monitoring of the grassland canopy recovery after burning should be considered at the species level. The same is valid for numerical vegetation models including plant competition, which can be initialized and validated using species-specific maps.

## Acknowledgment

The authors would like to thank Dr. D. Göttlicher and all students who support the flight operations, Naturaleza y Cultura Internacional (NCI) in Loja, for logistic support, the Ministry of the Environment of Ecuador (MAE) for the research permission (No.: 024-IC-AGUA-DPL-MA), and the two anonymous reviewers for improving the quality of this manuscript.

## References

[1] N. Brummitt and E. N. Lughadha, "Biodiversity: Where's hot and where's not ," *Conserv. Biol.*, vol. 17, no. 5, pp. 1442–1448, 2003.

[2] J. Bendix and E. Beck, "Spatial aspects of ecosystem research in a biodiversity hot spot of southern Ecuador—An introduction," *Erdkunde*, vol. 63, no. 4, pp. 305–308, 2009.

[3] D. Göttlicher *et al.*, "Land-cover classification in the Andes of southern Ecuador using Landsat ETM+ data as a basis for SVAT modelling," *Int. J. Remote Sens.*, vol. 30, no. 8, pp. 1867–1886, 2009.

[4] K. Roos, R. Rollenbeck, T. Peters, J. Bendix, and E. Beck, "Growth of tropical bracken (Pteridium arachnoideum): Response to weather variations and burning," *Invasive Plant Sci. Manage.*, vol. 3, no. 4, pp. 402–411, 2010.

[5] J. Bendix *et al.*, "Model parameterization to simulate and compare the PAR absorption potential of two competing plant species," *Int. J. Biometeorol.*, vol. 54, no. 3, pp. 283–295, 2010.

[6] B. Silva *et al.*, "Simulating canopy photosynthesis for two competing species of an anthropogenic grassland community in the Andes of southern Ecuador," *Ecol. Model.*, vol. 239, pp. 14–26, 2012.

[7] J. Bendix, R. Rollenbeck, D. Göttlicher, and J. Cermak, "Cloud occurrence and cloud properties in Ecuador," *J. Clim. Res.*, vol. 30, no. 2, pp. 133–147, 2006.

[8] C. Knoth, B. Klein, T. Prinz, and T. Kleinebecker, "Unmanned aerial vehicles as innovative remote sensing platforms for high-resolution infrared imagery to support restoration monitoring in cut-over bogs," *Appl. Veg. Sci.*, vol. 16, pp. 509–517, 2013.

[9] F. Artigas and I. C. Pechman, "Balloon imagery verification of remotely sensed Phragmites australis expansion in an urban estuary of New Jersey, USA," *Landscape Urban Plann.*, vol. 95, no. 3, pp. 105–112, 2010.

[10] M. Kamada and T. Okabe, "Vegetation mapping with the aid of low-altitude aerial photography," *Appl. Veg. Sci.*, vol. 1, no. 2, pp. 211–218, 1998.

[11] R. M. Larimer *et al.*, "Multispectral imaging systems on tethered balloons for optical remote sensing education and research," *J. Appl. Remote Sens.*, vol. 6, pp. 1–11, 2012.

[12] K. C. Swain and H. P. W. Jayasuriya, "Low altitude remote sensing applications for diversified farming conditions in developing countries: An overview," *Asia-Pacific J. Rural Develop.*, vol. 18, no. 2, pp. 81–98, 2008.

[13] J. S. Aber, "Lighter-than-air platforms for small-format aerial photography," *Trans. Kansas Acad. Sci.*, vol. 107, no. 1/2, pp. 39–44, 2004.

[14] D. Wundram and J. Löffler, "High-resolution spatial analysis of mountain landscapes using a low-altitude remote sensing approach," *Int. J. Remote Sens.*, vol. 29, no. 4, pp. 961–974, 2008.

[15] M. Miyamoto, K. Yoshino, T. Nagano, T. Ishida, and Y. Sato, "Use of balloon aerial photography for classification of Kushiro wetland vegetation, northeastern Japan," *Wetlands*, vol. 24, no. 3, pp. 701–710, 2004.

[16] R. M. Llovería, F. Perez-Cabello, A. García-Martín, and J. R. Fernández, "Combined methodology based on field spectrometry and digital photography for estimating fire severity," *IEEE J. Sel. Topics Appl. Earth Observ. Remote Sens.*, vol. 1, no. 4, pp. 266–274, Dec. 2008.

[17] X. Chen and L. Vierling, "Spectral mixture analyses of hyperspectral data acquired using a tethered balloon," *Remote Sens. Environ.*, vol. 103, no. 3, pp. 338–350, 2006.

[18] Y. Inoue, S. Morinaga, and A. Tomita, "A blimp-based remote sensing system for low-altitude monitoring of plant variables: A preliminary experiment for agricultural and ecological applications," *Int. J. Remote Sens.*, vol. 21, no. 2, pp. 379–385, 2000.

[19] L. A. Vierling, M. Fersdahl, X. Chen, Z. Li, and P. Zimmerman, "The short wave aerostat-mounted imager (SWAMI): A novel platform for acquiring remotely sensed data from a tethered balloon," *Remote Sens. Environ.*, vol. 103, no. 3, pp. 255–264, 2006.

[20] J. S. Aber, I. Marzolff, and J. B. Ries, *Small-Format Aerial Photography*. Amsterdam, The Netherlands: Elsevier, 2010, pp. 85–87.

[21] B. Planer-Friedrich, J. Becker, B. Brimer, and B. J. Merkel, "Low-cost aerial photography for high-resolution mapping of hydrothermal areas in Yellowstone National Park," *Int. J. Remote Sens.*, vol. 29, no. 6, pp. 1781–1794, 2008.

[22] D. G. Leckie *et al.*, "Automated tree recognition in old growth conifer stands with high resolution digital imagery," *Remote Sens. Environ.*, vol. 94, no. 3, pp. 311–326, 2005.

[23] L. T. Waser, C. Ginzler, M. Kuechler, E. Baltsavias, and L. Hurni, "Semi-automatic classification of tree species in different forest ecosystems by spectral and geometric variables derived from Airborne Digital Sensor (ADS40) and RC30 data," *Remote Sens. Environ.*, vol. 115, no. 1, pp. 76–85, 2011.

[24] A. B. Massada, O. Gabay, A. Perevolotsky, and Y. Carmel, "Quantifying the effect of grazing and shrub-clearing on small scale spatial pattern of vegetation," *Landscape Ecol.*, vol. 23, no. 3, pp. 327–339, 2008.

[25] J. P. Lesschen, L. H. Cammeraat, A. M. Kooijman, and B. van Wesemael, "Development of spatial heterogeneity in vegetation and soil properties after land abandonment in a semi-arid ecosystem," *J. Arid Environ.*, vol. 72, no. 11, pp. 2082–2092, 2008.

[26] H. T. Søgaard, "Weed classification by active shape models," *Biosyst. Eng.*, vol. 91, no. 3, pp. 271–281, 2005.

[27] M. D. Woebbecke, E. G. Meyer, K. Von Bargen, and A. D. Mortensen, "Shape features for identifying young weeds using image analysis," *Trans. ASAE*, vol. 38, no. 1, pp. 271–281, 1995.

[28] A. J. Perez, F. Lopez, J. V. Benlloch, and S. Christensen, "Colour and shape analysis techniques for weed detection in cereal fields," *Comput. Electron. Agric.*, vol. 25, no. 3, pp. 197–212, 2000.
[29] L. Tang, L. Tian, and B. L. Steward, "Classification of broadleaf and grass weeds using gabor wavelets and an artificial neural network," *Trans. ASAE*, vol. 46, no. 4, pp. 1247–1254, 2003.
[30] A. S. Laliberte and A. Rango, "Texture and scale in object-based analysis of subdecimeter resolution unmanned aerial vehicle (UAV) imagery," *IEEE Trans. Geosci. Remote Sens.*, vol. 47, no. 3, pp. 761–770, Mar. 2009.
[31] J. E. Taylor, "Factors causing variation in reflectance measurements from Bracken in Eastern Australia," *Remote Sens. Environ.*, vol. 43, no. 2, pp. 217–229, 1993.
[32] G. A. Blackburn and J. I. Pitman, "Biophysical controls on the directional spectral reflectance properties of bracken (Pteridium aquilinum) canopies: Results of a field experiment," *Int. J. Remote Sens.*, vol. 20, no. 11, pp. 2265–2282, 1999.
[33] G. A. Blackburn and C. M. Steele, "Towards the remote sensing of matorral vegetation physiology: Relationships between spectral reflectance, pigment, and biophysical characteristics of semiarid bushland canopies," *Remote Sens. Environ.*, vol. 70, no. 3, pp. 278–292, 1999.
[34] J. I. Pitman, "Absorption of photosynthetically active radiation, radiation use efficiency and spectral reflectance of bracken [Pteridium aquilinum (L.) Kuhnl] Canopies," *Ann. Bot.*, vol. 85, no. 2, pp. 101–111, 2000.
[35] G. F. Curatola Fernndez, B. Silva, J. Gawlik, B. Thies, and J. Bendix, "Bracken fern frond status classification in the Andes of southern Ecuador: Combining multispectral satellite data and field spectroscopy," *Int. J. Remote Sens.*, vol. 34, no. 20, pp. 7020–7037, 2013.
[36] J. M. Welles, "Some indirect methods of estimating canopy structure," *Remote Sens. Rev.*, vol. 5, no. 1, pp. 31–43, 1990.
[37] D. Göttlicher, J. Albert, T. Nauss, and J. Bendix, "Optical properties of selected plants from a tropical mountain ecosystem—Traits for plant functional types to parametrize a land surface model," *Ecol. Model.*, vol. 222, no. 3, pp. 493–502, 2011.
[38] N. Snavely, S. M. Seitz, and R. Szeliski, Photo tourism: Exploring photo collections in 3D, in *Proc. ACM SIGGRAPH 2006 Papers*, 2006, pp. 835–846.
[39] Grass Development Team, Geographic Resources Analysis Support System (GRASS) Software. (2012). *Open Source Geospatial Foundation Project* [Online]. Available: http://grass.osgeo.org
[40] J. Boehner, T. Selige, and A. Ringeler, "Image segmentation using representativeness analysis and region growing," in *SAGA–Analyses and Modelling Applications*, J. Boehner, K. R. McCloy and J. Strobl, Eds. Goettinger Geogr. Abh., 2006, vol. 115, pp. 29–38.
[41] G. Ridgeway. (Dec. 9, 2012). *Generalized Boosted Models: A Guide to the gbm Package* [Online]. Available: http://CRAN.R-project.org/package=gbm
[42] J. A. Richards and X. Jia, *Remote Sensing Digital Image Analysis: An Introduction*. New York, NY, USA: Springer-Verlag, 2005.
[43] D. Turner, A. Lucieer, and C. Watson, "An automated technique for generating georectified mosaics from ultra-high resolution unmanned aerial vehicle (UAV) imagery, based on structure from motion (sfm) point clouds," *Remote Sens.*, vol. 4, pp. 1392–1410, 2012.
[44] D. G. Lowe, "Distinctive image features from scale-invariant keypoints," *Int. J. Comput. Vis.*, vol. 60, no. 2, pp. 91–110, 2004.
[45] D. Rocchini *et al.*, "Robust rectification of aerial photographs in an open source environment," *Comput. Geosci.*, vol. 39, pp. 145–151, 2012.
[46] C. Straub and B. Koch, "Estimating single tree stem volume of Pinus sylvestris using airborne laser scanner and multispectral line scanner data," *Remote Sens.*, vol. 3, pp. 929–944, 2011.
[47] R. T. T. Forman, *Land Mosaics: The Ecology of Landscapes and Regions*. Cambridge, U.K.: Cambridge Univ. Press, 1995, ch. 4, pp. 141–142, 1995.
[48] R. M. Haralick, K. Shanmugam, and I. Dinstein, "Textural features for image classification," *IEEE Trans. Syst. Man Cybern.*, vol. SMC-3, no. 6, pp. 610–621, Nov. 1973.
[49] J. H. Friedman, "Greedy function approximation: A gradient boosting machine," *The Ann. Statist.*, vol. 29, no. 5, pp. 1189–1232, 2001.
[50] J. Elith, J. R. Leathwick, and T. Hastie, "A working guide to boosted regression trees," *J. Animal Ecol.*, vol. 77, no. 4, pp. 802–813, 2008.
[51] R Development Core Team. (Oct. 26, 2012). *R: A Language and Environment for Statistical Computing* [Online]. Available: http://www.R-project.org
[52] J. A. Hanley and B. J. McNeil, "The meaning and use of the area under a receiver operating characteristic (ROC) curve," *Radiology*, vol. 143, pp. 29–36, 1982.
[53] J. Pearce and S. Ferrier, "Evaluating the predictive performance of habitat models developed using logistic regression," *Ecol. Model.*, vol. 133, pp. 225–245, 2000.
[54] G. De'ath, "Boosted trees for ecological modeling and prediction," *Ecology*, vol. 88, pp. 243–251, 2007.

**Brenner Silva** (M'12) was born in Itajubá, Minas Gerais, Brazil, in 1977. He received the B.S. degree in computer science from the Federal University of Sao Carlos, São Carlos, Brazil, in 1999, the M.S. degree in remote sensing from the National Institute for Space Research (INPE), Sao José dos Campos, Brazil, in 2003, and the Ph.D. (Dr.rer.nat.) degree in geography from the Philipps University of Marburg, Marburg, Germany, in 2013.

From 2004 to 2007, he was a Research Assistant with the INPE, Professional in land surveying, and Spatial Analyst with regional and large-scale projects (e.g., PRODES, GEOMA, and PROBIO, funded by the Ministry of Environment of Brazil). Since 2008, he is with the Laboratory for Climatology and Remote Sensing at the Philipps University of Marburg, and until 2013, he was a member of the FOR816 research unit [National German Research Foundation (DFG)—BE1780/16-2]. His research interests include remote sensing, spatial analysis, and modeling of terrestrial systems.

Dr. Silva is a member of the "Platform for Biodiversity and Ecosystem Monitoring and Research in South Ecuador" (DFG—BE1780/38-1). He was a recipient of the Maria Sibylla Merian Award in the category Best Presentation Poster at the annual conference of the Society of Tropical Ecology, in 2014.

**Lukas Lehnert** received the B.S. degree in biology from the Philipps University of Marburg, Marburg, Germany, in 2009, and the Diploma degree in geography, in 2011, both from Philipps University of Marburg, Marburg, Germany.

Since 2011, he is a Research Assistant at the Laboratory for Climatology and Remote Sensing at the Philipps University of Marburg. His research interests include analyzing remotely sensed images of various scales in ecological applications.

**Kristin Roos** received the Diploma and Ph.D. degrees from the University of Bayreuth, Bayreuth, Germany, in 2004 and 2010, respectively.

She is a Biologist focusing on botany and genetics. From 2004 to 2014, she was a Research Associate with the Department of Plant Physiology, University of Bayreuth, Bayreuth, Germany. Her research interests include the restoration and sustainable management of pastures in the Andes of Ecuador.

Dr. Roos was a member of three DFG-financed research units FOR402 (BE473/31-3, from 2004 to 2007), FOR816 (BE473/38-1, from 2007 to 2010), and the prolongation of FOR816 (BE473/38-2, from 2010 to 2013). Since 2014, she has been a member of the Platform for Biodiversity and Ecosystem Monitoring and Research in South Ecuador. She was a recipient of the Merian Award of the Society for Tropical Ecology for her presentation at the annual conference 2008 in Hohenheim, Germany.

**Andreas Fries** received the M.S. degree (Dipl. Geographer) from the Ludwig-Maximilian University of Munich, München, Germany, in 2006, and the Ph.D. degree (Dr.rer.nat.) in geography from the Philipps University of Marburg, Marburg, Germany, in 2012.

From 2007 to 2008, he was a Technician with the Scientific Research Station San Francisco, Zamora, Ecuador, where he was in charge of the technical equipments of different research groups, investigating basic questions of climatology, ecology, and hydrology in a tropical mountain forest in South America. From 2008 to 2009, he had a 1-year granting by the DAAD (German Academic Exchange Service; D/07/48000), and from 2009 to 2012, he worked as an Associate Professor with the University of Loja, Loja, Ecuador (Universidad Tecnica Particular de Loja). Currently, he is a Research Assistant with the Laboratory for Climatology and Remote Sensing, Philipps University of Marburg and a Postdoc Member of the German Research Foundation (DFG) Transfer-Project "Operational rainfall monitoring in southern Ecuador" (BE 1780/31-1). His research interests include tropical climatology and impacts of deforestation on the local and regional climate.

**Rütger Rollenbeck** was born in Witten, Germany, in 1966. He received the Diploma degree from the University of Mannheim, Mannheim, Germany, in 1995, the Ph.D. degree from the Philipps University of Marburg, Marburg, Germany, in 2001, and the Post-doctoral degree in habilitation from the University of Marburg, Marburg, Germany, in 2011.

From 1995 to 1997, he worked as a Freelancer with the Brownfield Rehabilitation Industry. In 2000–2001, he supported the development of the AMAXDOAS sensor for EnviSat at the Institute for Environmental Physics, Heidelberg, Germany. Since 2001, he has been a Scientific Coordinator in several projects focused on climate dynamics and atmospheric chemistry within the DFG research units 402 and 816 and then has been a Professor of Geoecology and Climatology with the University of Marburg. Currently, he holds the position as Senior Scientist with the task of coordinating and managing data handling and archiving procedures for the "Platform for Biodiversity and Ecosystem Monitoring and research in Ecuador." His research interests include climatological processes, especially rainfall formation and climatic cycles.

**Erwin Beck** was born on November 2, 1937. He received the Dr.rer.nat. degree in plant systematics (with H. Merxmueller) from the University of Munich, München, Germany, in 1963.

In 1970, he worked as an Associate Professor with the Botanical Institute, University of Munich. From 1975 to 2006, he was a Full Professor and Head of the Department of Plant Physiology with the University of Bayreuth, Bayreuth, Germany. Since 1979, he is running research projects in the tropics. Since 2007, he is a Professor Emeritus at the University of Bayreuth. His research interests include plant (eco) physiology and molecular biology, plant hormone physiology, biodiversity research, vegetation ecology, and ecosystem theory.

Dr. Beck served the Academic as Dean of the Faculty, Vice-President of the University, and External Examiner of the University of Nairobi, Nairobi, Kenya, and of Addis Ababa University, Piazza, Addis Ababa, Ethiopia. He was elected as President of the German Biologists Association, President of the German Botanical Society, President of the German National Committee of the IUBS, and Treasurer of the IUBS. His honours are Order of Merit of the German Federal Republic, Professor Honoraria of the Universidad Técnica Particular de Loja (Ecuador), Dr.rer.nat. honoris causa from the Technical University of Kaiserslautern, Kaiserslautern, Germany, Honorary member of the German Botanical Society, and Associate member of the Ethiopian Academy of Science.

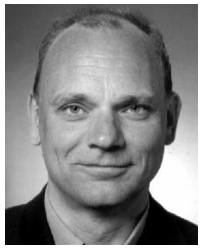

**Jörg Bendix** was born in Troisdorf-Sieglar, Germany, in 1961. He received the Diploma degree in geography (minors soil science and agricultural water engineering), in 1988, and the Ph.D. degree (Dr.rer.nat.) from the University of Bonn, Bonn, Germany, in 1992.

From 1988 to 1997, he worked as a Scientist with the University of Bonn, and, at the same time, in the working group "Geoecolgy" of the Academy of Science and Literature, Mainz, Germany. After his habilitation at the University of Bonn (in 1997), he worked as a Professor of Applied Physical Geography with the Ludwig-Maximilians-University Munich, Munich, Germany, in 1999. In 1997, he holds a Substitution Professorship for remote sensing with the University of Bonn and in 1998 for physical geography at the Philipps University of Marburg, Marburg, Germany. Currently, he is a Coordinator of an Interdisciplinary Research Group, the Platform for Biodiversity and Ecosystem Monitoring and Research in South Ecuador, Loja, Ecuador (http://www.tropicalmountainforest.org/). His research interests include climatology, atmospheric and land surface remote sensing, and ecological climatology.

Prof. Bendix is a member of the Academy of Science of Literature, Mainz, Germany, the German National Academy of Science, Leopoldina, Germany, the American Meteorological Society, and others. Since 2000, he holds the Chair for geoecolgy (specialization: climatology, remote sensing, and environmental modeling) with the Faculty of Geography, Philipps University of Marburg. He was a recipient of several national and international awards, e.g., the Kalkhof-Rose-Remembrance Award of the Academy of Science and Literature, Mainz, Germany.